Interfacial Exchange Coupling Induced Anomalous Anisotropic Magnetoresistance in Epitaxial γ'-Fe_4N/CoN Bilayers

Zirun Li[1], Wenbo Mi[1,a], Xiaocha Wang[2,b], Xixiang Zhang[3,c]

[1]*Tianjin Key Laboratory of Low Dimensional Materials Physics and Preparation Technology, Faculty of Science, Tianjin University, Tianjin 300072, China*

[2]*Tianjin Key Laboratory of Film Electronic & Communicate Devices, School of Electronics Information Engineering, Tianjin University of Technology, Tianjin 300384, China*

[3]*PSE Division, KAUST, Thuwal 23955-6900, Saudi Arabia*

ABSTRACT

Anisotropic magnetoresistance (AMR) of the facing-target reactively sputtered epitaxial γ'-Fe_4N/CoN bilayers is investigated. The phase shift and rectangular-like AMR appears at low temperatures, which can be ascribed to the interfacial exchange coupling. The phase shift comes from the exchange bias (EB) that makes the magnetization lag behind a small field. When the γ'-Fe_4N thickness increases, the rectangular-like AMR appears. The rectangular-like AMR should be from the combined contributions including the EB-induced unidirectional anisotropy, intrinsic AMR of γ'-Fe_4N layer and interfacial spin scattering.

Keywords: Anisotropic Magnetoresistance, Bilayer, Exchange Bias, Fe_4N, Facing-target Sputtering

■ INTRODUCTION

Interfacial interaction in the ferromagnetic/antiferromagnetic (FM/AFM) systems can lead to the exchange bias (EB).[1,2] The concrete manifestation of EB is the shift of the hysteresis loops. Considerable efforts have been devoted to understanding the physical picture of EB.[2,3] EB has been extensively studied for many decades and it is well known to the community that the interfacial exchange interaction can introduce higher order magnetic anisotropies in addition to the unidirectional one, most commonly another twofold anisotropy exist.[4-11] Unconventional fourfold anisotropy has been observed in the Co/FeF_2, Fe/MnF_2, NiFe/Fe_2O_3, NiFe/FeMn and FeMn/Co bilayers.[4-8] Even more the peculiar threefold and sixfold anisotropies in the FeNi/CoO bilayers have also been reported.[9] An exchange anisotropy in the Fe/MnF_2 bilayers has been observed including the unidirectional, uniaxial, threefold and fourfold symmetry components.[10] Besides, In the Fe/MnPd bilayers, the uniaxial and fourfold in-plane anisotropies cannot also be ignored.[11] Even though these higher order anisotropies induced by EB have been observed by magnetic measurements, no one reported how the anisotropies affect the anisotropic magnetoresistance (AMR).

We know that the hysteresis loop measurements are the common methods for investigating EB. However, Miller *et al.* reported a new technique, which uses the AMR to measure the exchange anisotropy in the EB systems.[12,13] The presence of EB

will affect the angular-dependent AMR due to the pinned magnetic moments.[14] Generally, AMR is observed in the ferromagnetic materials due to the spin-orbit coupling.[15] If θ_M is the angle between the magnetization and current, the resistivity is defined as $\rho(\theta_M) = \rho_\perp + (\rho_\mathrm{P} - \rho_\perp)\cos^2\theta_M$, where ρ_P ($\rho_\perp$) is the resistivity where current is parallel (perpendicular) to magnetization. In EB systems, when rotating the external field to an angle θ with respect to current, $\rho(\theta)$ does not follow a simple $\cos^2\theta$ dependence. Thus, it is interesting to investigate AMR in EB systems.

We have studied the EB of the epitaxial γ'-Fe_4N/CoN bilayers by measuring its hysteresis loop.[16] In this work, we report the AMR of the γ'-Fe_4N/CoN bilayers. Negative AMR and twofold symmetry are observed in the single γ'-Fe_4N epitaxial films.[17] However, in the epitaxial γ'-Fe_4N/CoN bilayers, the rectangular-like AMR and phase shift appear, which is ascribed to the interfacial exchange coupling.

■ EXPERIMENTAL DETAILS

Epitaxial γ'-Fe_4N(t nm)/CoN(8 nm) bilayers were fabricated on MgO(100) substrates using DC reactive facing-target sputtering. CoN(8 nm) films were deposited on the γ'-Fe_4N films with different thicknesses t from 6 to 20 nm. During facing-target sputtering, the substrate will be free from the bombardment of high-energy particles.[18,19] Therefore, the large-area uniformity, low substrate temperature and

relatively free of inert incorporation of the facing-target sputtered films can be realized, which may reduce the interfacial interdiffusion that is beneficial for the fabrication of bilayers.[18,19] Details for the epitaxial growth of γ'-Fe_4N films were referred to our period work.[20] CoN layers were grown by sputtering from a pair of pure Co targets (4N) in a 2.0-Pa pure N_2 (5N). The substrate was kept at 150 ^oC and sputtering power was 28 W. The film thickness was determined using a Veeco Dektak 6M surface profiler and confirmed by FEI Tecnai G2 F20 transmission electron microscopy (TEM). The microstructure was obtained by Rigaku D/max–2500 X-ray diffraction (XRD) and TEM. The magnetic properties were measured by using a Quantum Design superconducting quantum interference device (SQUID). AMR was measured using a Quantum Design physical property measurement system (PPMS). AMR ratio was defined as

$$\mathrm{AMR} = (\rho - \rho_{\max}) / \rho_{\max}, \quad (1)$$

where ρ_{max} is the maximum resistivity while the magnetic field rotates in the film plane.

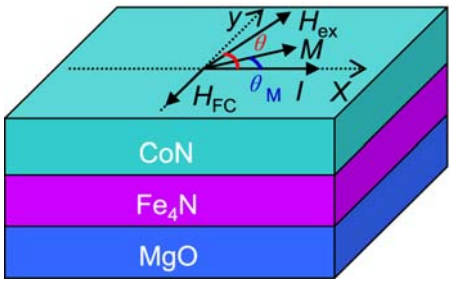

Figure 1. A schematic drawing of the cooling field H_{FC}, external field H_{ex}, magnetization M and current I.

During the measurements, the samples were cooled to 3 K under a 50-kOe field that was parallel to the film plane. Magnetic field was rotated clockwise from 0^o to 360^o and then anticlockwise to the original position by monitoring ρ as a function of θ. A schematic drawing of the cooling field H_{FC}, external field H_{ex}, magnetization M and current I was shown in Figure 1.

■ RESULTS AND DISCUSSION

In our previous work, the XRD results reveal that γ'-Fe_4N(200) layers epitaxially grows on MgO(100), then CoN(111) sits on γ'-Fe_4N(200) lattice. The epitaxial relation is MgO(100)||γ'-Fe_4N(100)||CoN(111) and MgO[100]||γ'-Fe_4N[$1\bar{1}0$]||CoN[$1\bar{1}0$].[16]

Figure 2a shows the low-magnification cross-sectional TEM image of the

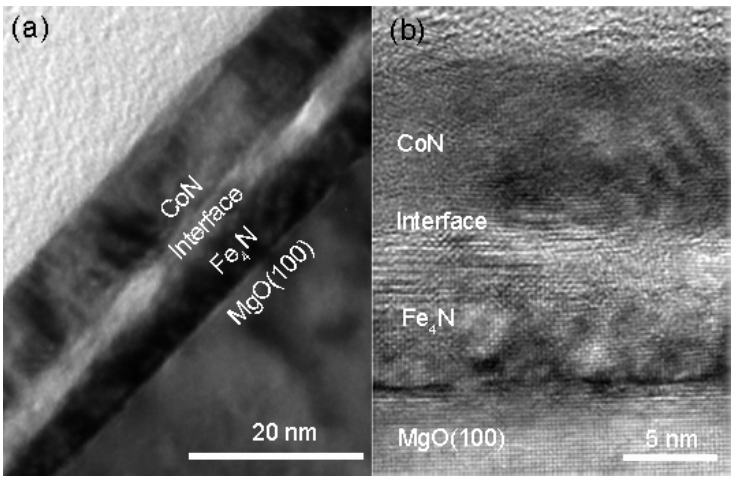

Figure 2. (a) low-magnification and (b) high-resolution cross-sectional TEM images of the γ'-Fe_4N(8 nm)/CoN(8 nm) bilayer.

γ'-Fe_4N/CoN bilayer. Both the thicknesses of γ'-Fe_4N and CoN layers are ~8 nm, confirming that determined by Dektak 6M surface profiler. The high-resolution TEM image in Figure 2b reveals the sharp interfaces between MgO and γ'-Fe_4N, as well as between γ'-Fe_4N and CoN. The sharp interfaces are beneficial for the study of EB.

Figures 3a-e present the hysteresis loops of the γ'-Fe_4N(t nm)/CoN(8 nm) bilayers at 3 K. An obvious loop shift appears due to EB. As the γ'-Fe_4N thickness decreases, EB shows a roughly increased tendency. At t=6 nm, EB has a maximum value of 410 Oe. The loop shape is not as smooth as the other samples and 1-kOe field is not large enough to saturate the magnetization. The unsmooth loop should be related to various complex and disordered magnetic structures due to the strong exchange coupling at t=6 nm.[16] Domain model may be used to explain the unsmooth loops.[16] The FM domain size in the γ'-Fe_4N(6 nm) layer is so small that the interaction between the domains can introduce an additional pinning effect. The interaction competes with other energies, thus leads to the formation of new domain structures during the magnetization reversal. The loop shift and coercivity depend on the reversal processes, so both EB and coercivity significantly increases.[16]

Figures 3f-j show the AMR curves of the γ'-Fe_4N(t nm)/CoN(8 nm) bilayers at 3 K and 0.5 kOe. The field cooling process is the same as that in the hysteresis loop measurements. We first notice that at t=6 nm the most obvious EB appears, and only one minimum in AMR occurs around 250°, breaking the $\cos^2\theta$ dependence. This

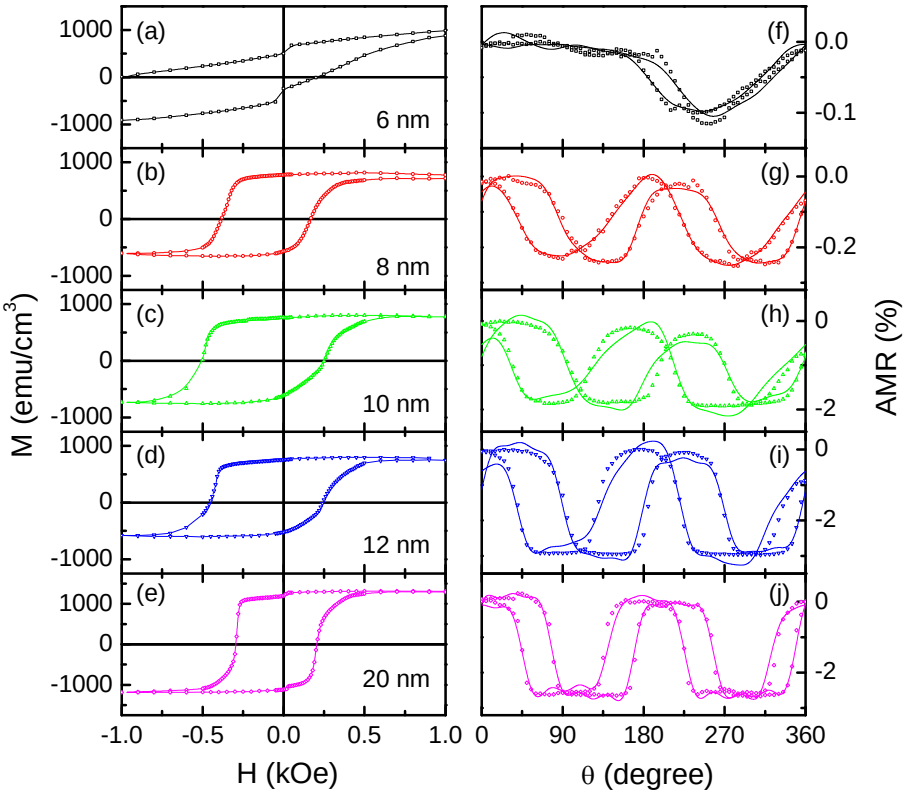

Figure 3. Hysteresis loops of the γ'-Fe_4N(t nm)/CoN(8 nm) bilayers with different t at 3 K, (a) 6 nm, (b) 8 nm, (c) 10 nm, (d) 12 nm, (e) 20 nm; (f)-(j) are the corresponding AMR curves at 3 K and 0.5 kOe. Solid lines are the fitted curves by equation (2).

indicates that the magnetization remains pinned along EB direction because the 0.5-kOe field is not large enough to break the exchange coupling.[14] At t=8 nm, AMR can be described by a $\cos^2\theta$ dependence, but an obvious hysteresis appears as the magnetization is dephased with respect to the appield small field. The phase shift verifies the pinning effect. With the increased t, the phase shift always exists.

However, it is noteworthy that AMR curve gradually transforms into a rectangular

shape as t increases, especially at t=20 nm. The deviation from the $\cos^2\theta$ dependence implies that magnetization rotation in the γ'-Fe_4N layer is dominated by the interfacial interaction. For confirming the interfacial effects, we need to exclude the influence of the single γ'-Fe_4N and CoN layer. The AMR curves of single γ'-Fe_4N layer at different temperatures are shown in Figure 4a. It is found that a good twofold symmetry without rectangular-like shape appears. In addition, the systematic AMR measurements for the single γ'-Fe_4N layer with different film thicknesses and external fields have been performed in ref. 17. The AMR of the epitaxial single γ'-Fe_4N films with different thicknesses from 5 to 58 nm reveals a good twofold symmetry.[17] Under different

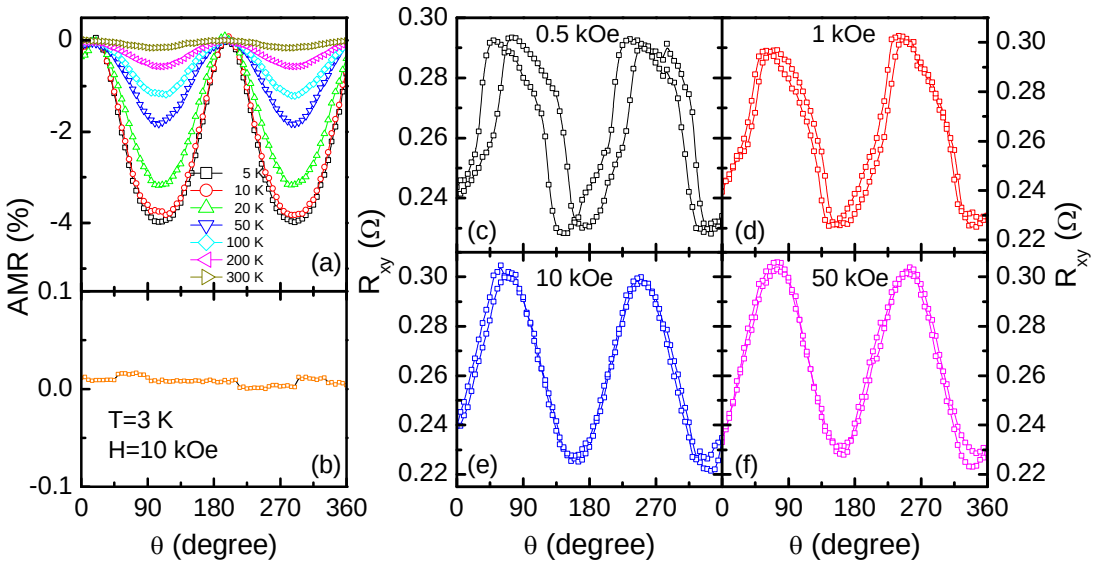

Figure 4. (a) AMR of γ'-Fe_4N(26 nm) film with 10-kOe magnetic field at different temperatures; (b) AMR of CoN(22 nm) film with 10-kOe magnetic field at 3 K; (c)-(f) are the angular dependent planar Hall effect (PHE) of γ'-Fe_4N(20 nm)/CoN(8 nm) bilayer at 10 K with different magnetic fields.

external fields from 0.5 to 50 kOe, the AMR of the epitaxial γ'-Fe_4N films also shows a twofold symmetry and no deviation from $\cos^2\theta$ dependence.[17] The AMR of the single CoN layer is almost a straight line, as shown in Figure 4b, which should not contribute to the rectangular-like AMR. Therefore, we can conclude that the rectangular-like AMR is from the interfacial effects of the bilayers.

As t increases, the pinning effect becomes weak. This weakened magnetic coupling leads to a slight disorder of the interfacial spins. The interfacial spin scattering may induce the additional anisotropy in γ'-Fe_4N layer. According to the Fourier transform, the rectangular wave can be broken up into many cosine waves. Therefore, the superimposition of multiple cosine functions may lead to the rectangular-like AMR. To confirm the speculation, we try to fit the AMR curves using Fourier transform formula. Finally, the AMR curves are well fitted using the following equation of

$$\mathrm{AMR} = C_0 + C_1\cos\theta + C_2\cos 2\theta + C_4\cos 4\theta + C_6\cos 6\theta + C_8\cos 8\theta + C_{10}\cos 10\theta \quad (2)$$

where C_0 is a constant, and C_1, C_2, C_4, C_6, C_8, and C_{10} are the Fourier coefficients of $\cos\theta$, $\cos 2\theta$, $\cos 4\theta$, $\cos 6\theta$, $\cos 8\theta$, and $\cos 10\theta$ components, respectively. The solid lines in Figures 3f-j are the fitted curves by using equation (2). The fitted Fourier coefficients are summarized in Table 1, which will be discussed in details.

In general, AMR in ferromagnets is supposed to be twofold symmetric and only $\cos 2\theta$ dependence is considered. However, C_4 appears in the single γ'-Fe_4N films at

Table 1. The Fourier coefficients obtained by fitting equation (2) for the γ'-Fe_4N(t nm)/CoN(8 nm) bilayers at 3 K.

t (nm)	C_1	C_2	C_4	C_6	C_8	C_{10}
6	-0.04735	-0.02074	0.00545	-0.00100	-0.00083	-0.00025
8	0.01808	-0.12696	0.00816	0.01786	-0.00291	-0.00370
10	-0.34190	-0.83647	0.16916	0.12607	0.03094	-0.00999
12	-0.23906	-1.70600	0.03526	0.34198	-0.03118	0.11033
20	0.13460	-1.64651	0.08065	0.41655	-0.04900	-0.18030

low temperatures, which is induced by the crystal field splitting due to the tetragonal lattice distortion.[21-23] The AMR of the single γ'-Fe_4N epitaxial films has been discussed.[17] At low temperatures, the AMR curves of single γ'-Fe_4N films contain not only cos2θ term but also cos4θ component.[17] Fourier coefficient C_2 and C_4 strongly depend on the measuring temperatures. With the increase of temperature, C_4 disappears rapidly. The appearance of C_4 at low temperatures is attributed to the crystal field splitting of d orbitals induced by the lattice changes.[17] In the γ'-Fe_4N/CoN bilayers, the lattice compression at low temperatures causes the tetragonal lattice distortion, so C_4 appears. The twofold and fourfold anisotropies induced by EB may contribute to C_2 and C_4, but their roles are small compared with the intrinsic AMR of γ'-Fe_4N layer.

The meaning of other coefficients may be speculated from the comparisons. Firstly, it is important to note that C_1 cannot be neglected at t=6 nm. If we set C_1=0, the

AMR curves cannot be fitted using the remaining coefficients. As shown in Table 1, in all the coefficients at t=6 nm, C_1 is the largest one, meaning that the contribution of C_1 is the largest, even larger than C_2. At t=6 nm, EB is the largest, so the existence of C_1 may be from the large unidirectional anisotropy of EB. With the increased t, C_1 contribution reduces. This variation trend is consistent with EB, further confirming that cosθ component comes from the contribution of EB. Recently, Cui *et al.* report that EB has a significant influence on the magnetization reorientation in two dimension.[24] When EB is comparable with the applied field, AMR exhibits the periodicity of 360^0 with a cosθ dependence. The symmetry-breaking is considered that the total vector of EB and applied field determines the magnetization direction,[24] which just confirms our viewpoints that EB induces the cosθ component.

With the increased t, the rectangular-like AMR appears. According to Fourier transform with the coefficients of C_1, C_2 and C_4, the rectangular wave is unable to form by the superimposition of these three cosine functions. Some reports show that the exchange coupling can induce the high order anisotropy contributions.[4-11, 25] So the higher order terms should play a significant role on AMR. In Table 1, C_6 occupies an increasing proportion as t increases. At t=12 and 20 nm, C_6 ranks the second one and exceeds C_1. Meanwhile, C_8 and C_{10} also gradually increase. By comparison, the increase of C_6 is the most obvious, C_{10} comes the second, C_8 is the weakest. With the increased t, C_1 reduces while the higher order terms increase. The reduction of C_1

implies the weakened EB. These two opposite changes indicate that the appearance of higher order terms should be from the weakened EB. The weakened pinning effect makes the interfacial spins become slight disordered, so the interfacial spin scattering enhances and the higher order terms are induced by the interfacial spin scattering.

For clarifying the origin of unusual AMR, we also measured the planar Hall effect (PHE). PHE is also an effective method to characterize the exchange anisotropy in EB systems.[26] So the γ'-Fe_4N(20 nm)/CoN(8 nm) bilayer was cooled under the same conditions with AMR measurements. When measuring PHE, the applied rotating field is along the sample plane. The results are shown in Figures 4c-f. Under a 0.5 kOe field, the phase shift appears, which suggests that EB can also affect PHE.[27] With the increased magnetic field, the phase shift disappears. But the rectangular-like shape is not observed in PHE, which is different from AMR. The traditional explanation of AMR and PHE is the change of scattering rate with the angle θ. Hu *et al.* and Li *et al.* observed the different symmetry in AMR and PHE in Fe_3O_4 and $La_{2/3}Ca_{1/3}MnO_3$ films, respectively.[28,29] They found that AMR has a transition from twofold to fourfold symmetry, while PHE only shows a $\sin 2\theta$ dependence. They explain the distinction according to the original resistivity tensor formula.[28,29] Considering the vanished matrix elements due to cubic symmetry and Onsager relation, the in-plane longitudinal resistivity ρ_{xx} (AMR) and transverse resistivity ρ_{xy} (PHE) can be expressed as[28]

$$\rho_{xx} = C'_0 + C'_1 \cos^2\theta + C'_2 \cos^4\theta + \cdots, \quad (3)$$

$$\rho_{xy} = C'_4 \sin\theta\cos\theta \quad (4)$$

Obviously, AMR contains the twofold and fourfold symmetry terms, even higher order terms, whereas PHE only contains twofold symmetry term. So the change of symmetry appears in AMR, but does not happen in PHE. Now we consider AMR and PHE in the γ'-Fe_4N/CoN bilayers using the above explanation. By comparison, it is found that EB leads to the appearance of hysteresis in AMR and PHE. Meanwhile, EB will break the symmetry of γ'-Fe_4N layer and induced the higher order terms in AMR, thus the rectangular-like AMR appears. However, PHE just relies on the twofold symmetry, it follows $\sin 2\theta$ relation and no rectangular shape appears.

Now we try to explain the physical mechanism of higher order terms. Generally, the higher-order coefficients are fairly small as compared with C_2 and are negligible. However, in the γ'-Fe_4N/CoN bilayers, twofold symmetry is broken and AMR shows rectangular. So we have to reconsider them. Three factors are crucial for the rectangular-like AMR: (1) The unidirectional anisotropy induced by EB will introduce $\cos\theta$ term; (2) The intrinsic twofold and fourfold symmetry caused by crystal field splitting in the γ'-Fe_4N layer are the major parts of AMR; (3) Interfacial spin scattering leads to the additional anisotropy, which is the key to higher order terms. With the increased t, the $\cos\theta$ contribution decreases, the intrinsic AMR of γ'-Fe_4N layer maintains, and the contribution of the interfacial spin scattering increases.

For further understanding the rectangular-like AMR, the different magnetic fields

are applied to measure AMR at t=20 nm and 3 K, as shown in Figures 5a-f. The solid lines are the fitting ones. When the magnetic field increases, the phase shift decreases. The large magnetic field results in the synchronous rotation of magnetization. So above 5 kOe, the phase shift disappears. However, AMR still remains the rectangular-like shape. Although the magnetic field is large enough to saturate the magnetization, the exchange coupling at 3 K still remains, which confirming that the interfacial coupling is responsible for the rectangular-like AMR.

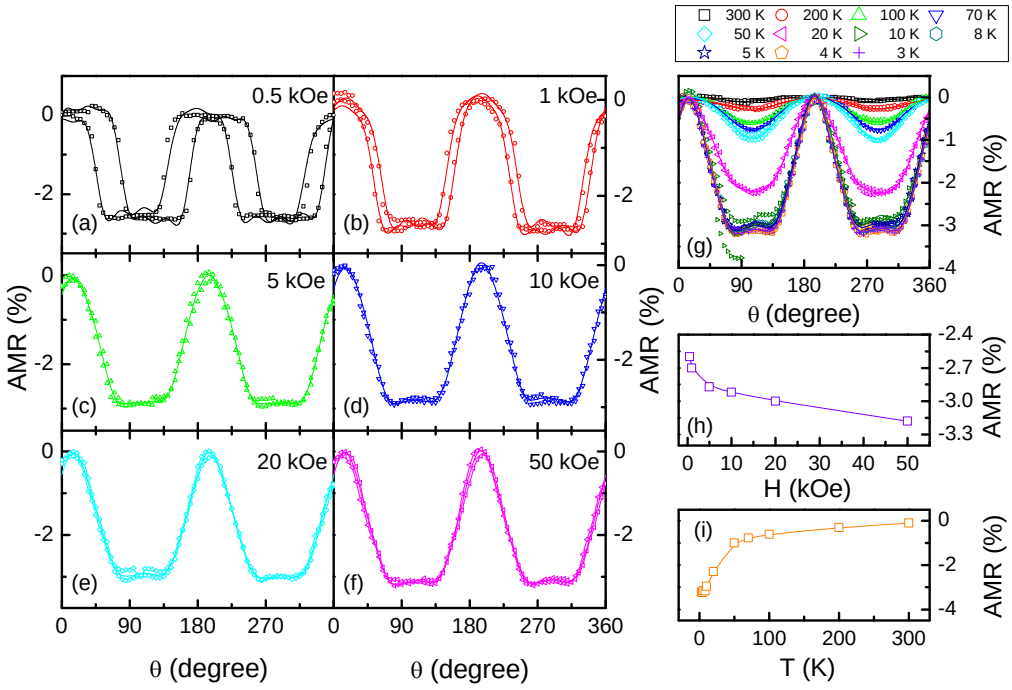

Figure 5. (a)-(f) are AMR curves of the γ'-Fe_4N(20 nm)/CoN(8 nm) bilayer under different magnetic fields at 3 K; (g) AMR of the γ'-Fe_4N(20 nm)/CoN(8 nm) bilayer at 50 kOe and different temperatures, the solid lines are the fitted curves by equation (2); (h) Magnetic-field dependent AMR at 3 K; (i) Temperature-dependent AMR of at 50-kOe field.

Figure 5g gives the AMR curves of the γ'-Fe_4N(20 nm)/CoN(8 nm) bilayer at different temperatures. The AMR can be well fitted by equation (2). Only a slight deviation from $\cos^2\theta$ dependence appears at low temperatures. As temperature increases, the rectangular-like AMR transforms into the cosine curve at 20 K due to the decreased exchange interaction. The recovery of cosine curve with the increased temperature suggests that the rectangular-like AMR is really depended on the interfacial exchange coupling. In Figure 5h, as the magnetic field increases, the absolute value of AMR gradually increases. In Figure 5i, with the increase of temperature, AMR decreases rapidly, which can be ascribed to the introduction of phonon scattering.

■ CONCLUSION

we have observed that the obvious phase shift and rectangular-like AMR appear in the epitaxial γ'-Fe_4N/CoN bilayers. Phase shift corresponds with EB variation because the pinning effect makes the magnetization lag behind the small external field. The rectangular-like AMR may be from the competition of various contributions including EB-induced unidirectional anisotropy, the intrinsic AMR of γ'-Fe_4N and interfacial spin scattering.

■ AUTHOR INFORMATION

Corresponding Author

[a]E-mail: miwenbo@tju.edu.cn

[b]E-mail: wangxccn@126.com

[c]E-mail: xixiang.zhang@kaust.edu.sa

Author Contributions

All of the authors designed the experiments and outline of the manuscript; Z.L. and W.M. performed the experiments and wrote the main manuscript text; X.W. and X.Z. contributed detailed discussions and revisions. All authors reviewed the manuscript.

Notes

The authors declare no competing financial interest

■ ACKNOWLEDGEMENTS

This work is supported by the National Natural Science Foundation of China (51171126), Key Project of Natural Science Foundation of Tianjin City (12JCZDJC27100 and 14JCZDJC37800), Program for New Century Excellent Talents in University (NCET-13-0409) and Scientific Research Foundation for the Returned Overseas Chinese Scholars, State Education Ministry.

■ REFERENCES

(1) Meiklejohn, W. H.; Bean, C. P. New Magnetic Anisotropy. *Phys. Rev.* **1956**, *102*, 1413-1414.

(2) Nogués, J.; Schuller, I. K. Exchange Bias. *J. Magn. Magn. Mater.* **1999**, *192*, 203-232.

(3) Nogués, J.; Sort, J.; Langlais, V.; Skumryev, V.; Suriñach, S.; Muñoz, J. S.; Baró, M. D. Exchange Bias in Nanostructures. *Phys. Rep.* **2005**, *422*, 65-117.

(4) Grimsdith, M.; Hoffmann, A.; Vavassori, P.; Shi, H.; Lederman, D. Exchange-Induced Anisotropies at Ferromagnetic-Antiferromagnetic Interfaces above and below the Néel Temperature. *Phys. Rev. Lett.* **2003**, *90*, 257201.

(5) Pechan, M. J.; Bennett, D.; Teng, N.; Leighton, C.; Nogués, J.; Schuller, I. K. Induced Anisotropy and Positive Exchange Bias: A Temperature, Angular, and Cooling Field Study by Ferromagnetic Resonance. *Phys. Rev. B* **2002**, *65*, 064410.

(6) Bali, R.; Stelmashenko, N. A.; Blamire, M. G. Exchange Bias and Fourfold Magnetic Anisotropy in Permalloy Thin Film on Epitaxial Hematite Antiferromagnet. *J. Appl. Phys.* **2008**, *103*, 053911.

(7) Mewes, T.; Hillebrands, B.; Stamps, R. L. Induced Fourfold Anisotropy and Bias in Compensated NiFe/FeMn Double Layers. *Phys. Rev. B* **2003**, *68*, 184418.

(8) Chen, G.; Li, J.; Liu, F. Z.; Zhu, J.; He, Y.; Wu, J.; Qiu, Z. Q.; Wu, Y. Z. Four-Fold

Magnetic Anisotropy Induced by the Antiferromagnetic Order in FeMn/Co/Cu(001) System. *J. Appl. Phys.* **2010**, *108*, 073905.

(9) Radu, F.; Mishra, S. K.; Zizak, I.; Erko, A. I.; Dürr, H. A.; Eberhardt, W.; Nowak, G.; Buschhorn, S.; Zabel, H.; Zhernenkov, K.; Wolff, M.; Schmitz, D.; Schierle, E.; Dudzik, E.; Feyerherm, R. Origin of the Reduced Exchange Bias in an Epitaxial FeNi(111)/CoO(111) Bilayer. *Phys. Rev. B* **2009**, *79*, 184425.

(10) Krivorotov, I. N.; Leighton, C.; Nogués, J.; Schuller, I. K.; Dahlberg, E. D. Relation Between Exchange Anisotropy and Magnetization Reversal Asymmetry in Fe/MnF_2 Bilayers. *Phys. Rev. B* **2002**, *65*, 100402(R).

(11) Tang, Y. J.; Roos, B. F. P.; Mewes, T.; Frank, A. R.; Rickart, M.; Bauer, M.; Demokritov, S. O.; Hillebrands, B.; Zhou, X.; Liang, B. Q.; Chen, X.; Zhan, W. S. Structure and Magnetic Properties of Exchange-Biased Polycrystalline Fe/MnPd Bilayers. *Phys. Rev. B* **2000**, *62*, 8654-8657.

(12) Miller, B. H.; Dahlberg, E. D. Use of the Anisotropic Magnetoresistance to Measure Exchange Anisotropy in Co/CoO Bilayers. *Appl. Phys. Lett.* **1996**, *69*, 3932-3934.

(13) Gredig, T.; Krivorotov, I. N.; Dahlberg, E. D. Magnetization Reversal in Exchange Biased Co/CoO Probed with Anisotropic Magnetoresistance. *J. Appl. Phys.* **2002**, *91*, 7760-7762.

(14) Laukhin, V.; Skumryev, V.; Martí, X.; Hrabovsky, D.; Sánchez, F.; García-Cuenca,

M. V.; Ferrater, C.; Varela, M.; Lüders, U.; Bobo, J. F.; Fontcuberta, J. Electric-Field Control of Exchange Bias in Multiferroic Epitaxial Heterostructures. *Phys. Rev. Lett.* **2006**, *97*, 227201.

(15) McGuire, T. R.; Potter, R. I. Anisotropic Magnetoresistance in Ferromagnetic 3*d* Alloys. *IEEE Trans. Magn.* **1975**, *11*, 1018-1038.

(16) Li, Z. R.; Mi, W. B.; Wang, X. C.; Bai, H. L. Inversion of Exchange Bias and Complex Magnetization Reversal in Full-Nitride Epitaxial γ'-Fe_4N/CoN Bilayers. *J. Magn. Magn. Mater.* **2015**, *379*, 124-130.

(17) Li, Z. R.; Feng, X. P.; Wang, X. C.; Mi, W. B. Anisotropic Magnetoresistance in Facing-Target Reactively Sputtered Epitaxial γ'-Fe_4N Films. *Mater. Res. Bull.* DOI: 10.1016/j.materresbull.2015.01.053.

(18) Lin, C.; Sun, D. C.; Ming, S. L.; Jiang, E. Y.; Liu, Y. G. Magnetron Facing Target Sputtering System for Fabricating Single-Crystal Films. *Thin Solid Films* **1996**, *279*, 49-52.

(19) Noda, K.; Hirata, T.; Kawanabe, T.; Naoe, M. Novel Facing Targets Sputtering Apparatus with Uniform Magnetic Field and Plasma-Free Substrates. *Vaccum* **1998**, *51*, 687-690.

(20) Mi, W. B.; Guo, Z. B.; Feng, X. P.; Bai, H. L. Reactively Sputtered Epitaxial γ'-Fe_4N Films: Surface Morphology, Microstructure, Magnetic and Electrical Transport Properties. *Acta Mater.* **2013**, *61*, 6387-6395.

(21) Kabara, K.; Tsunoda, M.; Kokado, S. Annealing Effects on Nitrogen Site Ordering and Anisotropic Magnetoresistance in Pseudo-Single-Crystal γ'-Fe_4N Films. *Appl. Phys. Express* **2014**, *7*, 063003.

(22) Ito, K.; Kabara, K.; Sanai, T.; Toko, K.; Imai, Y.; Tsunoda, M.; Suemasu, T. Sign of the Spin-Polarization in Cobalt-Iron Nitride Films Determined By the Anisotropic Magnetoresistance Effect. *J. Appl. Phys.* **2014**, *116*, 053912.

(23) Ito, K.; Kabara, K.; Takahashi, H.; Sanai, T.; Toko, K.; Suemasu, T.; Tsunoda, M. Negative Anisotropic Magnetoresistance in γ'-Fe_4N Epitaxial Films on $SrTiO_3$(001) Grown by Molecular Beam Epitaxy. *Jpn. J. Appl. Phys.* **2012**, *51*, 068001.

(24) Cui, B.; Song, C.; Sun, Y.; Wang, Y. Y.; Zhao, Y. L.; Li, F.; Wang, G. Y.; Zeng, F.; Pan, F. Exchange Bias Field Induced Symmetry-Breaking of Magnetization Rotation in Two-Dimension. *Appl. Phys. Lett.* **2014**, *105*, 152402.

(25) Kim, J. V.; Stamps, R. L.; McGrath, B. V.; Camley, R. E. Angular Dependence and Interfacial Roughness in Exchange-Biased Ferromagnetic/Antiferromagnetic Bilayers. *Phys. Rev. B* **2000**, *61*, 8888-8894.

(26) Lu, Z. Q.; Pan, G.; Lai, W. Y. Planar Hall Effect in NiFe/NiMn Bilayers. *J. Appl. Phys.* **2001**, *90*, 1414-1418.

(27) Barzola-Quiquia, J.; Lessig, A.; Ballestar, A.; Zandalazini, C.; Bridoux, G.; Bern, F.; Esquinazi, P. Revealing the Origin of the Vertical Hysteresis Loop Shifts in an Exchange Biased Co/$YMnO_3$ Bilayer. *J. Phys. Condens.: Matter* **2012**, *24*, 366006.

(28) Hu, C. R.; Zhu, J.; Chen, G.; Li, J. X.; Wu, Y. Z. Direct Comparison of Anisotropic Magnetoresistance and Planar Hall Effect in Epitaxial Fe_3O_4 Thin Films. *Phys. Lett. A* **2012**, *376*, 3317-3321.

(29) Li, J.; Li, S. L.; Wu, Z. W.; Li, S.; Chu, H. F.; Wang, J.; Zhang, Y.; Tian, H. Y.; Zheng, D. N. A Phenomenological Approach to the Anisotropic Magnetoresistance and Planar Hall Effect in Tetragonal $La_{2/3}Ca_{1/3}MnO_3$ Thin Films. *J. Phys. Condens.: Matter* **2010**, *22*, 146006.

■ Table of Contents Graphic (TOC)